Imaging the Activity and Localization of Single Voltage-Gated Ca^{2+} Channels by Total Internal Reflection Fluorescence Microscopy

Angelo Demuro and Ian Parker
Department of Neurobiology and Behavior, University of California, Irvine, California

ABSTRACT The patch-clamp technique has enabled functional studies of single ion channels, but suffers limitations including lack of spatial information and inability to independently monitor currents from more than one channel. Here, we describe the use of total internal reflection fluorescence microscopy as an alternative, noninvasive approach to optically monitor the activity and localization of multiple Ca^{2+}-permeable channels in the plasma membrane. Images of near-membrane Ca^{2+} signals were obtained from >100 N-type channels expressed within restricted areas (80 × 80 μm) of *Xenopus* oocytes, thereby permitting simultaneous resolution of their gating kinetics, voltage dependence, and localization. Moreover, this technique provided information inaccessible by electrophysiological means, demonstrating that N-type channels are immobile in the membrane, show a patchy distribution, and display diverse gating kinetics even among closely adjacent channels. Total internal reflection fluorescence microscopy holds great promise for single-channel recording of diverse voltage- and ligand-gated Ca^{2+}-permeable channels in the membrane of neurons and other isolated or cultured cells, and has potential for high-throughput functional analysis of single channels.

INTRODUCTION

Recent developments in optical technology have made it possible to image the activity of individual ion channels (Zou et al., 1999, 2002; Wang et al., 2001; Sonnleitner et al., 2002; Sonnleitner and Isacoff, 2003; Borisenko et al., 2003; Demuro and Parker, 2003). Such approaches have promise as an adjunct to the well-established patch-clamp technique for single-channel recording (Hamill et al., 1981), and have particular advantages over electrophysiological techniques in that they provide spatial information of channel locations, permit simultaneous recording from multiple channels, and are applicable to channels that are inaccessible to a patch-clamp pipette.

Much interest has focused on imaging Ca^{2+}-permeable channels (Zou et al., 1999, 2002; Wang et al., 2001; Demuro and Parker, 2003)—largely because the enormous changes in local cytosolic Ca^{2+} concentration during channel openings together with the availability of highly sensitive fluorescent Ca^{2+} indicators provide much larger optical signals than can be obtained from probes that directly sense conformational changes in channel proteins (Sonnleitner et al., 2002; Sonnleitner and Isacoff, 2003). To obtain optimal signal/noise ratio and kinetic resolution it is necessary to monitor Ca^{2+}-dependent fluorescence from a region as close as possible to the channel mouth. Ca^{2+} concentration changes in this vicinity closely track the opening and closing of the channel, whereas diffusion of Ca^{2+} away from the local microdomain both dilutes the signal at increasing distances and slows its kinetics. Wide-field imaging by conventional epifluorescence microscopy therefore provides only a limited temporal resolution of channel activity (~100 ms: Zou et al., 1999, 2002). Instead, the best results to date have been obtained using confocal microscopy, where fluorescence is monitored from a subfemtoliter volume (Wang et al., 2001; Demuro and Parker, 2003). However, there are practical limitations as to how fast the confocal laser spot can be scanned, which have necessitated a tradeoff between spatial and temporal resolution. Prior studies have, therefore, used line-scan imaging, in which fluorescence is monitored along only a single line in the cell, typically scanned every 2–8 ms. This has significant disadvantages in that spatial information is highly restricted, only a few channels may lie close to the scan line, and out-of-focus signals arise from channels to either side of the scan.

To circumvent these limitations we explored the use of total internal reflection fluorescence microscopy (TIRFM) for rapid two-dimensional imaging of single channel cytosolic Ca^{2+} signals arising very close the cell membrane. The principle and application of TIRFM have been extensively reviewed (Toomre and Manstein, 2001; Axelrod, 2003), and the technique has previously been applied to image near-membrane Ca^{2+} signals—although not with single channel resolution (Cleeman et al., 1997; Becherer et al., 2003; Zenisek et al., 2003). TIRFM works by directing excitation light through a glass substrate toward an aqueous specimen at a sufficiently shallow angle that total internal reflection occurs due to the refractive index decrease at the glass/water interface. However, a very thin electromagnetic field (evanescent wave) is created in the liquid with the same wavelength as the incident light, and decays exponentially with distance from the interface (typically over one or a few hundred nm). This field is able to excite fluorophores near the interface while avoiding excitation further into the aqueous phase, and thus provides an ''optical sectioning'' effect similar to, but even narrower, than that achieved by a confocal microscope. Moreover, the plane of fluorescence

Submitted November 7, 2003, and accepted for publication December 16, 2003.

Address reprint requests to I. Parker, E-mail: iparker@uci.edu.

0006-3495/04/05/3250/10 $2.00

excitation can be directly imaged by a camera, permitting two-dimensional visualization at a speed limited only by the frame rate of the camera or by the availability of sufficient emitted photons to provide adequate signal/noise ratio.

Here, we employed TIRFM to image Ca^{2+} flux through individual N-type voltage-gated Ca^{2+} channels expressed in *Xenopus* oocytes, and demonstrate the utility of this approach as a practicable means to simultaneously monitor the functional gating properties and spatial localization of numerous single channels.

MATERIALS AND METHODS

Oocyte preparation and electrophysiology

Experiments were performed on defolliculated stage V and VI oocytes obtained from *Xenopus laevis* (Demuro and Parker, 2003). Plasmids containing cDNA clones coding for the N-type Ca^{2+} channel $\alpha_{1B\text{-}d}$ and β_3 subunits were linearized and transcribed in vitro (Lin et al., 1997), and equal quantities of each subunit cRNA were mixed to a final concentration of 0.1–1 $\mu g/\mu l$ and injected (50 nl) into oocytes. After 3–5 days we assayed the expression of voltage-gated N-type channels by voltage-clamp recording of Ca^{2+}-dependent Cl^- currents (T_{out}) (Miledi and Parker, 1983) evoked by depolarization to +30 mV in 6 mM Ca^{2+} Ringer's solution. Oocytes showing currents >3 μA were selected for imaging, and were injected ~1 h before use with fluo-4-dextran (MW 10,000 D; k_D for Ca^{2+} ~3 μM) to a final intracellular concentration of ~40 μM. Fluo-4 was chosen as the indicator because it shows a large (>30-fold) maximal increase on binding Ca^{2+}, and the dextran conjugate minimized compartmentalization problems observed with the free indicator. Oocytes were then transferred to a hypertonic stripping solution (composition: K-aspartate, 200 mM; KCl, 20 mM; $MgCl_2$, 1 mM; EGTA, 10 mM; HEPES, 10 mM: pH 7.2), allowing the vitelline envelope to be carefully torn apart and removed using a pair of fine forceps (Methfessel et al., 1986). Finally, oocytes were transferred to high-Ca^{2+} Ringer's solution (composition: NaCl, 110 mM; $CaCl_2$, 6 mM, KCl, 2 mM; HEPES, 5 mM; at pH 7.2) and placed animal hemisphere down in a recording chamber formed by cementing an O-ring onto a fresh microscope cover glass. The membrane potential was clamped at holding potentials of −60 or −80 mV using a two-electrode voltage-clamp (Gene Clamp 500, Axon Instruments, Foster City, CA), and stepped to more positive potentials to induce opening of N-type Ca^{2+} channels expressed in the plasma membrane.

TIRFM imaging

Imaging was accomplished using a home-built TIRF microscope system (Parker, 2003), illustrated schematically in Fig. 1 *A*. In brief, this was based around an Olympus IX 50 microscope (modified for use with infinity-corrected objectives) equipped with an Olympus 60× TIRFM objective (NA = 1.45). Excitation light from the expanded beam of an argon ion laser (488 nm) was reflected by a dichroic mirror and brought to a focus at the rear focal plane of the objective. Translation of the focusing lens (*FL*; Fig. 1 *A*) allowed the beam to be introduced either at the extreme edge of the objective aperture (for TIR excitation), or more centrally (for wide-field) excitation. Initial adjustment of the microscope for TIRFM imaging was accomplished using a dilute suspension of 100-nm diameter fluorescent beads in water (Fluorospheres, Molecular Probes, Engene, OR). When FL was adjusted for TIR excitation only those beads that had adhered to the cover glass and become immobile were visible, whereas mobile beads undergoing Brownian motion in the water also became visible when the laser beam entered the more central part of the objective aperture. An adjustable rectangular aperture (*A*; Fig. 1 *A*) placed at a conjugate image plane in the excitation path restricted the illuminated area to ~80 × 80 μm at the specimen, and the aperture was overfilled by collimated laser light emerging from a beam expander to provide Koehler illumination. Emitted fluorescence was collected through the same objective and, after passage through barrier filters (>510 nm to block 488-nm laser excitation and >650 nm to block infrared emission from the laser tube), was imaged using a Gen. 3 image intensifier tube coupled through a relay lens to a digital video camcorder (Canon Elura, Canon USA, Lake Success, NY). Image data were recorded at video rate (30 frames s^{-1}) on mini digital video tapes for offline digitization and analysis using the MetaMorph software package (Universal Imaging, Westchester, PA). An electronic shutter blocked the laser beam except when imaging and its opening was synchronized by a computer that also applied depolarizing pulses via the voltage-clamp.

RESULTS

TIRFM imaging of oocytes

After allowing a vitelline-stripped oocyte to settle for a few minutes on the cover glass forming the base of the imaging chamber, we searched for regions that showed a fairly uniform, dim resting fluorescence when viewed by TIRFM. Many oocytes were rejected because they failed to show fluorescence (even though appearing bright by wide-field excitation), suggesting that they had not adhered sufficiently well to bring the cytosol within the evanescent layer; or because they showed extensive, bright fluorescence reflecting a high Ca^{2+} level due to membrane damage. Moreover, we restricted analysis to regions near the edge of the adherent membrane patch, so as to minimize problems from depletion of Ca^{2+} in the thin layer of extracellular solution trapped between the oocyte and the cover glass and possible loss of voltage control owing to the high extracellular series resistance of this thin fluid layer. To compensate for variations in fluorescence across the imaging field—due both to patterning of the coherent laser beam and irregularities in spacing between the oocyte membrane and cover glass—we present images and measurements as the ratio ($\Delta F/F$) of the fluorescence change on stimulation (ΔF) relative to the resting fluorescence (F) at the same pixel averaged over several video frames. At holding potentials negative to ~−40 mV the resting fluorescence was usually stationary, but in some cases we observed spontaneous local transients that may reflect basal activity of an unknown type of channel endogenously present in the oocyte membrane (Demuro and Parker, 2003). These events could readily be distinguished because they dimmed during depolarization, and were excluded from analysis.

Imaging Ca^{2+} influx through single voltage-gated channels

Depolarization of oocytes expressing voltage-gated N-type Ca^{2+} channels to potentials more positive than ~−20 mV resulted in the sporadic appearance of numerous, transient bright spots in the TIRFM image (Supplementary Video; Figs. 1 *C* and 3 *A*). Based on previous evidence from

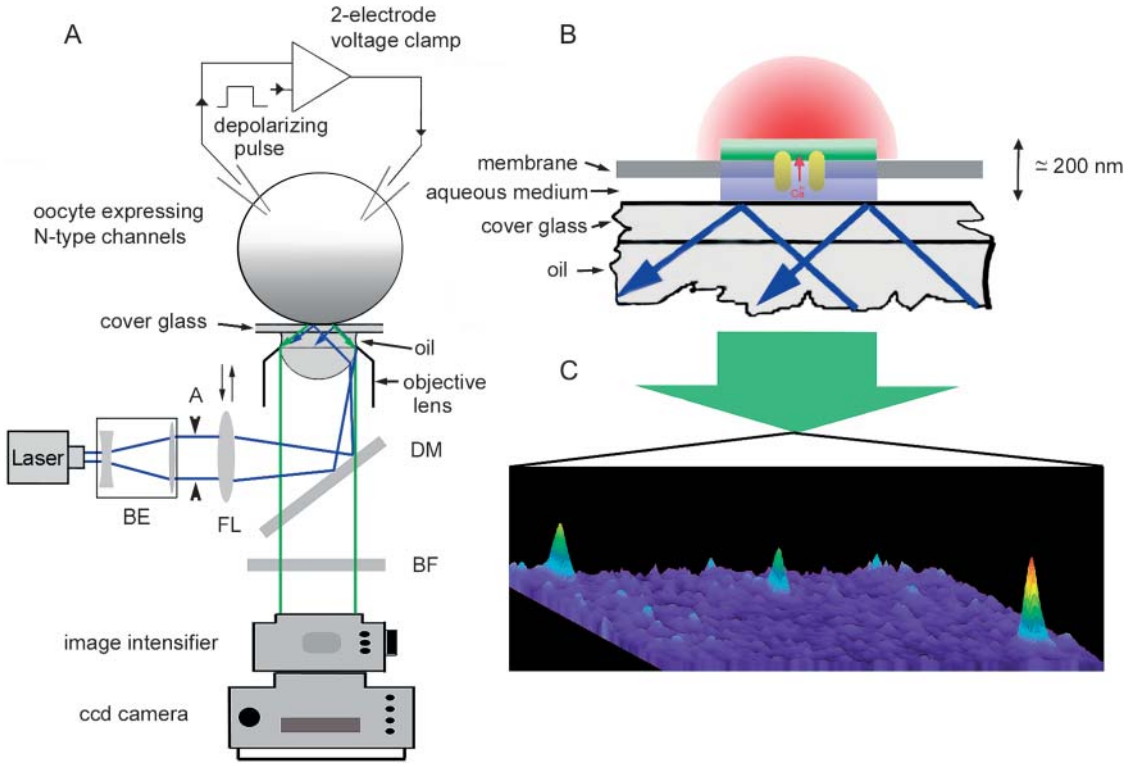

FIGURE 1 Imaging single-channel Ca^{2+} signals by total internal reflection fluorescence microscopy. (*A*) Schematic of the TIRFM imaging system. The 488-nm beam from an argon ion laser (50 mW) passes through a 5× beam expander (*BE*) and is focused by a lens (*FL*; $f = 150$ mm) via a dichroic mirror (*DM*) to a spot at the back focal plane of the microscope objective lens (Olympus TIRFM 60×, oil immersion, $NA = 1.45$). The focusing lens is mounted on a micrometer-driven translation stage, so that the laser beam can be adjusted to enter the periphery of the objective aperture so as to achieve total internal reflection at the interface between the cover glass and the aqueous bathing medium. An adjustable rectangular knife-blade aperture (*A*) located at a conjugate image plane defines the field of excitation. Fluorescence excited in the specimen by the evanescent wave is collected by the same objective, passes through the dichroic mirror and a barrier filter (*BF*) blocking the laser wavelength, and is imaged by an intensifier tube coupled through a relay lens to a charge-coupled device camera. An oocyte expressing N-type channels is loaded with fluo-4 dextran, stripped of its vitelline envelope and allowed to adhere (animal hemisphere down) to a cover glass forming the base of the imaging chamber. Its membrane potential is controlled by a two-electrode voltage-clamp. (*B*) Schematic, illustrating the imaging of near-membrane fluorescent Ca^{2+} signals near an open channel by TIRFM. (*C*) Single video frame obtained by TIRFM illustrating Ca^{2+} signals from simultaneous opening of three channels within an 80 × 80-μm patch of oocyte membrane in response to depolarization to −15 mV. Increasing $[Ca^{2+}]$ is denoted both by ''warmer'' colors and by height.

confocal imaging (Demuro and Parker, 2003), and results presented here, we interpret these sparklets to arise from Ca^{2+} flux through individual N-type voltage-gated channels.

As illustrated in Fig. 2, the resolution of these events was greatly improved by TIRFM imaging as compared to wide-field fluorescence microscopy. Sparklets visualized by TIRFM were spatially restricted (<1 μm), and fluorescence measurements obtained from a small (5 × 5 pixel; 0.9 × 0.9 μm) region of interest centered on a sparklet showed large fluorescence signals ($\Delta F/F > 1$) with good signal/noise ratio and rapid kinetics (Fig. 2 *A*). In contrast, images obtained from the same channel after adjusting the laser beam to achieve wide-field fluorescence excitation showed more diffuse and dimmer signals, making it difficult or impossible to identify discrete events in fluorescence records (Fig. 2 *B*).

The imaging field encompassed a roughly 80 × 80 μm region of the oocyte membrane, within which we often observed sparklets arising at >100 discrete sites. It was thus possible to monitor the simultaneous activity of numerous channels. For example, Fig. 3 shows representative records of simultaneous activity from 40 channels during a single depolarizing pulse.

Voltage-dependence of single-channel and macroscopic Ca^{2+} signals

We examined the voltage-dependence of Ca^{2+} signals by TIRFM imaging while applying depolarizing pulses to various potentials. As illustrated in Fig. 4 *A*, depolarization to ~−30 mV evoked only a few sparklets, whereas the numbers of sites showing sparklets at any given time increased steeply with increasing depolarization. Measurements of total Ca^{2+} influx (derived as a spatial average of peak fluorescence throughout the entire imaging field) showed a biphasic voltage-dependence (Fig. 4 *B*), increasing progressively between ~−40 mV and +60 mV, and then

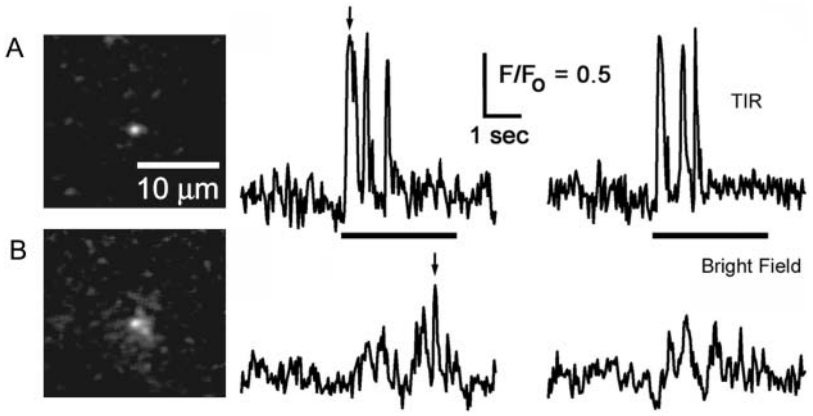

FIGURE 2 TIRFM enhances resolution of single-channel Ca^{2+} signals by providing a thin optical section. (*A*) TIRFM image shows fluorescence at the peak of a sparklet, and traces show two examples of fluorescence signals monitored from a 0.9 × 0.9 μm region centered on this sparklet in response to successive depolarizing pulses from −80 mV to −10 mV. Arrow marks the time at which the image was captured and bars indicate depolarizing pulses. (*B*) Corresponding image and fluorescence traces obtained from the same channel after adjusting the laser beam for conventional wide-field epifluorescence excitation.

declining to zero at ~+100 mV. This is expected to reflect two processes—voltage-dependent gating of N-type channels leading to an increasing number of open channels at more positive voltages, and a reduction in single-channel Ca^{2+} flux as the potential approaches the (very positive) Ca^{2+} equilibrium potential. To separate these effects, we measured the fluorescence amplitudes of individual sparklets (Fig. 4 *C*), and the frequency of sparklets (Fig. 4 *D*). Sparklet amplitude decreased at increasingly positive voltages, as expected from the reduced electrochemical driving force for Ca^{2+} flux through individual plasma membrane channels. Conversely, sparklet frequency (a measure of opening probability) was almost zero at voltages negative to ~−30 mV, but then increased steeply with depolarization,

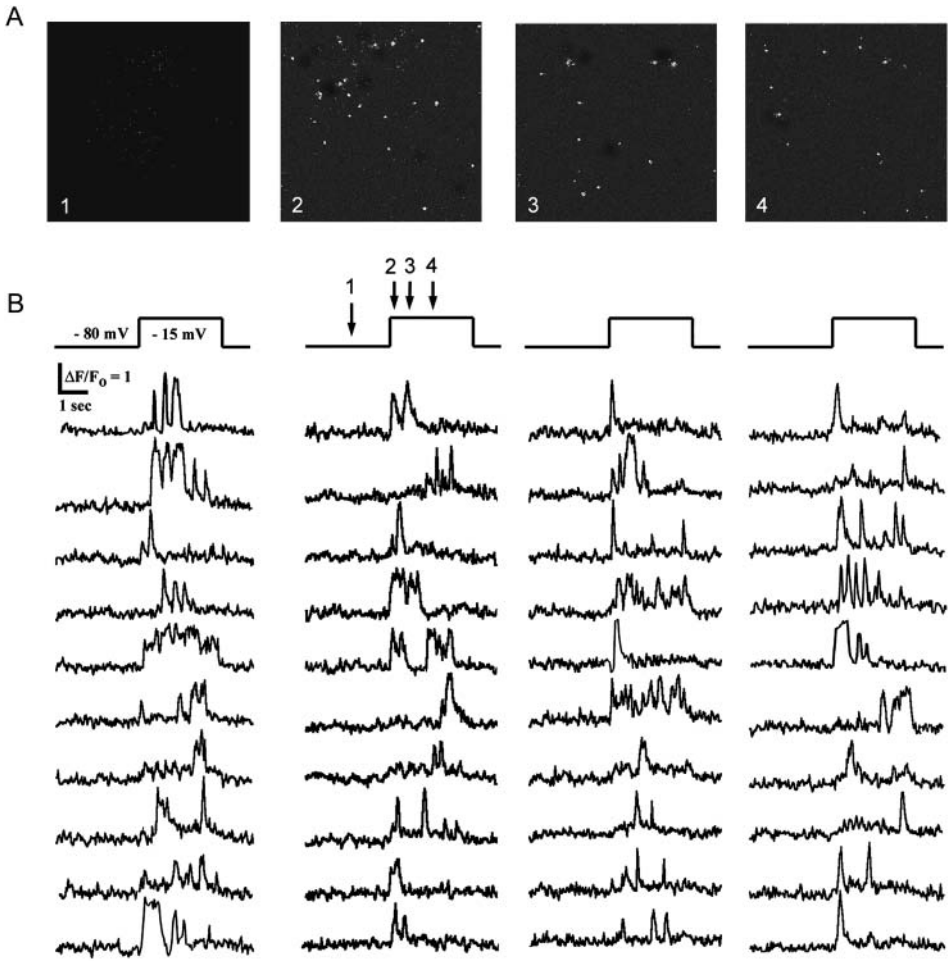

FIGURE 3 Simultaneous optical recording from numerous N-type channels within an imaging field. (*A*) Sequence showing representative TIRFM images captured before and at different times (indicated by *numbered arrows* in *B*) after depolarizing the oocyte to −15 mV. Each image is a single video frame, and shows sparklets arising at several channels throughout the field. (*B*) Traces show fluorescence signals recorded simultaneously during a single depolarizing pulse from independent regions of interest (~1 μm^2) placed over 40 channels.

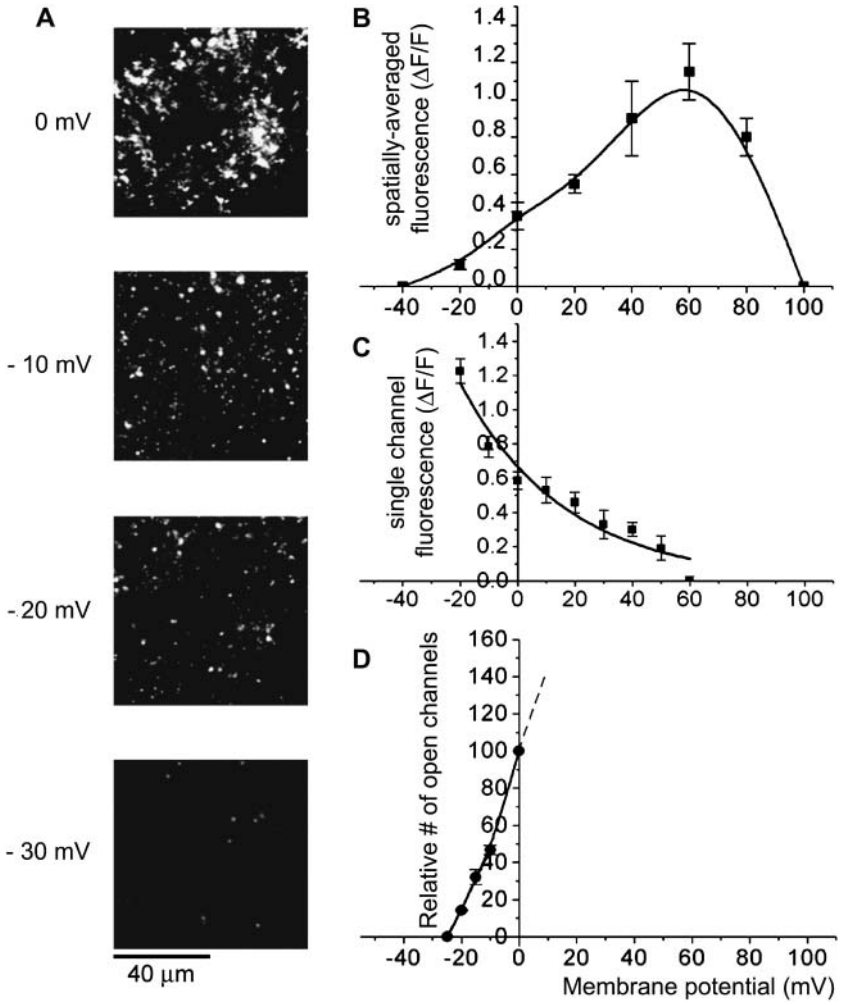

FIGURE 4 Voltage-dependence of macroscopic and single-channel TIRFM Ca^{2+} signals. (*A*) Panels show representative single video frames of TIRFM images from a given patch of oocyte membrane captured 100 ms after depolarizing from −80 mV to the various potentials indicated. (*B*) Voltage dependence of macroscopic Ca^{2+} signal. Graph plots the mean fluorescence increase ($\Delta F/F$) averaged over the entire image field as a function of membrane potential. Measurements were made during the first 300 ms of each depolarizing pulse, and data are mean ± SEM of measurements from six observations. (*C*) Voltage dependence of fluorescence signal during individual sparklets. Data are measurements of local fluorescence measured from 1 μm^2 regions of interest centered on individual channels ($n = 11$). (*D*) Voltage dependence of frequency of channel openings. Measurements were made by counting the number of discrete sparklets occurring throughout the imaging field during the first 200 ms after onset of depolarization to various voltages. Points show mean numbers of openings ($n = 5$ trials), scaled relative to that at 0 mV. Data could not be obtained at positive voltages, as the high frequency of events precluded reliable identification of individual sparklets.

consistent with voltage-dependent gating of N-type channels (Lin et al., 1997).

Channel gating kinetics

To explore the utility of TIRFM for analysis of channel kinetics we imaged >200 sparklets during depolarization to −20 mV. Their durations varied widely between 33 ms (a single video frame) and several hundred ms, and followed a single exponential distribution with a time constant of 64 ms (Fig. 5 *A*) consistent with Markovian channel gating. There was, however, a falloff in observations with durations <50 ms, and the time constant was slower than we had previously measured (28 ms) using line-scan confocal microscopy to image sparklets from the same N-type channels. In comparison, patch-clamp measurements of Ba^{2+} currents through single N-type channels expressed in oocytes gave an even shorter mean open time (~12 ms; Demuro and Parker, 2003). These discrepancies likely reflect the temporal limitations of the optical recordings (33 ms per frame with the video-rate camera used in the present studies), which would attenuate brief closings so that measurements of sparklet durations reflect that of bursts of openings, rather than their constituent openings (Demuro and Parker, 2003).

The frequency of occurrence of sparklets was greatest immediately after onset of depolarization, and then declined exponentially with a time constant of 1.36 s (Fig. 5 *B*). This mirrors the inactivation kinetics of the channels, and qualitatively matches the decline of whole-cell Ba^{2+} currents recorded under voltage-clamp in oocytes expressing N-type channels (Demuro and Parker, 2003), although quantitative differences may be expected using Ba^{2+} as the charge carrier.

Spatial spread of fluorescence signal

Fig. 6 *A* shows the mean spatial spread of fluorescence measured diametrically through sparklets at the time of peak amplitude. This is fit well by a Gaussian curve with a width (full-width at half-maximum amplitude; i.e., FWHM) of 0.71 μm. It was thus possible to spatially resolve simultaneous sparklets at adjacent sites as close as ~700 nm, and the centroid of individual sparklets could be determined with

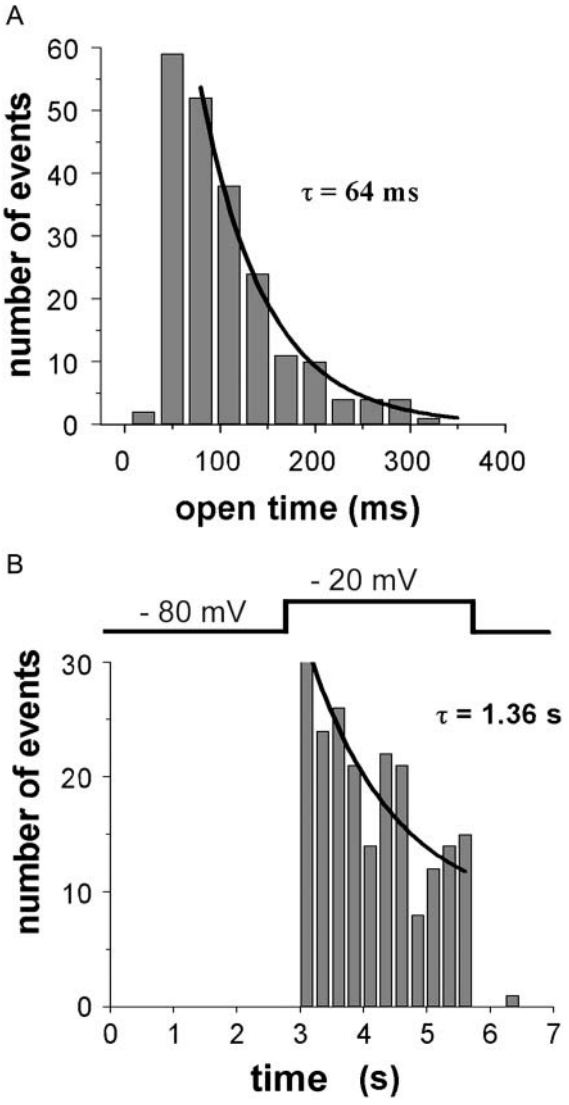

FIGURE 5 Kinetics of sparklets. (*A*) Histogram shows distribution of durations of sparklets, measured at half maximal amplitude. Fitted curve is a single exponential with time constant of 64 ms. Data are from 243 events, $n = 40$ channels. (*B*) Decline in opening frequency during sustained depolarization. Histogram bars show the numbers of sparklets observed during successive 0.25-s time bins at a holding potential of −80 mV before and after depolarization, and throughout a 3-s depolarization to −20 mV as indicated. Data are from 40 channels. Fitted curve is a single exponential with a time constant of 1.36 s.

appreciably better precision (limited by signal/noise consideration, but in practice <200 nm).

It should be noted that the spatial distribution of the fluorescence signal does not directly reflect the underlying gradient of free [Ca^{2+}], and that the latter will be more tightly restricted that the observed sparklet. Firstly, the sparklets are appreciably blurred by the point-spread function of the microscope (~0.45 μm; see Fig. 6 *B*). Secondly, Ca^{2+}-bound indicator molecules are able to diffuse readily in the cytoplasm, whereas the motility of Ca^{2+} ions is restricted by binding to immobile buffers (Allbritton et al, 1992).

As illustrated in Fig. 6, *D* and *E*, the signal amplitude decayed rapidly with increasing distance away from the center of a sparklet, and the temporal resolution declined such that brief events were grossly attenuated at a radial distance of only 1 μm. Thus, an optimal signal/noise ratio and kinetic resolution was achieved by monitoring fluorescence from a region of interest (0.27 μm radius) corresponding roughly to the microscope point-spread function.

Restricted lateral motility of N-type channels

The fact that sparklets could be recorded over periods of several minutes from small (1 μm^2) regions at fixed positions already suggested that N-type channels showed little or no lateral mobility in the oocyte membrane. To further examine this point, we tracked the centroid positions of sparklets over time. Fig. 7 shows an example where sparklets were evoked at a fixed site by two trains of depolarizing pulses, delivered ~4 min apart. Any change in position over this time was <0.5 μm, likely within the range of measurement error. By comparison, the effective diffusion coefficient for freely motile proteins within a planar lipid bilayer is ~3 $\mu m^2\ s^{-1}$ (Edidin, 1987; Borisenko et al., 2003), so by random motion a channel would be expected to move a mean distance of >50 μm in 270 s. Thus, N-type channels appear to be rigidly anchored in the oocyte membrane.

Moreover, a relatively homogeneous distribution of channels would be expected if they were able to undergo free lateral distribution, whereas we observed a markedly patchy distribution, with some regions of the oocyte membrane showing a high density of channels whereas other regions of the same oocyte showed few or no channels (Fig. 8 *A*). This variation in channel density does not appear to arise artifactually as a result of patchy adhesion of the oocyte membrane to the glass, because the observed channel density was not obviously correlated with any variation in resting background fluorescence (an indicator of proximity to the cover glass). Furthermore, confocal line-scan imaging of oocytes surrounded by an intact vitelline envelope showed a similar patchy distribution and lack of channel mobility (Demuro and Parker, 2003).

Differences in gating kinetics between channels

The ability to image simultaneously the activity of numerous channels makes it possible to map their localization with submicrometer resolution, and to compare the gating kinetics of channels within a given region of membrane. For example, Fig. 8 *B* maps the positions of 72 channels within the imaging field, and encodes a measure of their open probability by using a color scale to indicate the number of sparklets observed at each site in response to 10 successive depolarizing pulses. Considerable variation was apparent in

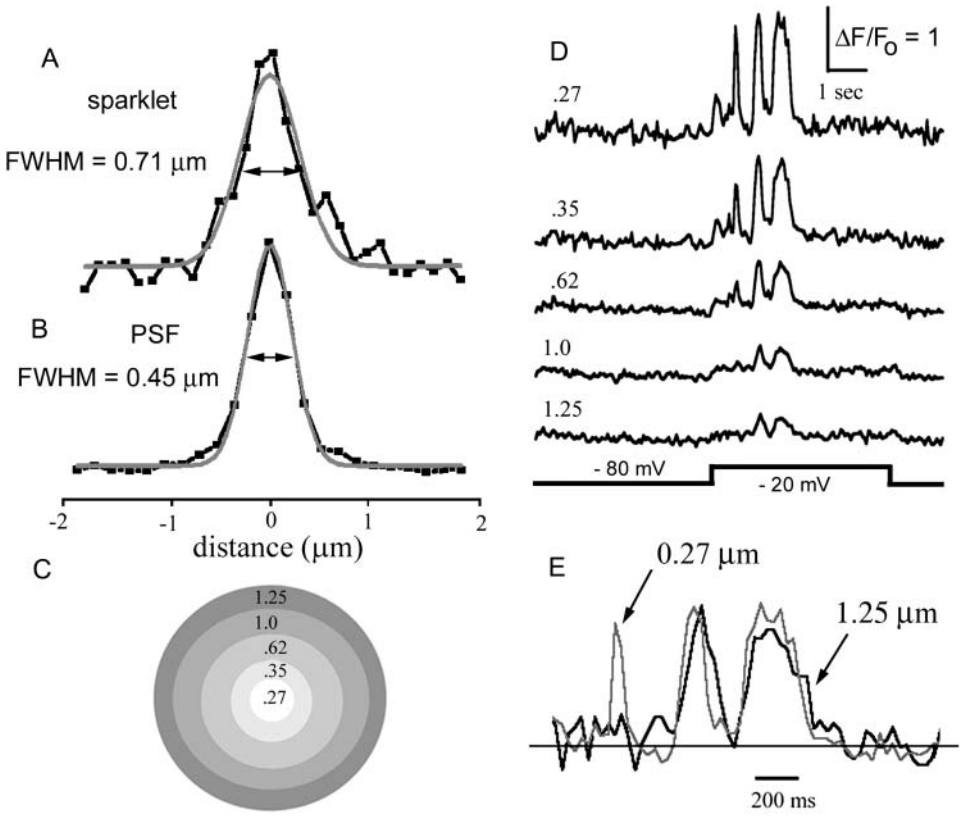

FIGURE 6 Spatial spread and kinetics of fluorescence signal during sparklets. (*A*) Radial distribution of fluorescence intensity across the sparklet. Dark trace shows the mean of fluorescence measurements made across a line (width 0.5 μm) passing diametrically through images of nine sparklets, each captured as a single video frame at the time of peak fluorescence. Shaded curve is a fitted Gaussian with width (FWHM) = 0.71 μm. (*B*) Corresponding fluorescence profile and Gaussian fit (FWHM = 0.45 μm) obtained using a 100-nm diameter fluorescent bead to measure the lateral point-spread function of the microscope. (*C*) Schematic, illustrating annular regions centered on a channel used to measure the traces in *D*. Scale corresponds to that in *A* and *B*, and numbers indicate mean radial distance (in μm) of each annular ring from the center. (*D*) Traces show fluorescence signals measured from these different annular rings during a depolarizing pulse that evoked several sparklets at a single channel. (*E*) Superposition of records from a spot (0.27 μm radius) centered on the channel and an annular ring of radius 1.25 μm around the channel. Traces are normalized to the same peak value to facilitate comparison of kinetic differences.

sparklet frequency between different channels, with some showing a total of only one or two events, whereas others showed 20 or more sparklets (Fig. 8 *C*). Overall, the distribution of mean opening frequencies among the 72 channels followed a decaying curve, with many channels giving infrequent sparklets, and progressively fewer displaying higher frequencies (*red histogram*, Fig. 8 *D*).

Because channel gating is stochastic, considerable statistical variation is expected during relatively short records like those in Fig. 8 *C*. To test whether this factor alone could account for the observed spread of sparklet frequencies we calculated the Poissonian distribution predicted if all channels displayed a probability equal to the population mean (0.685 sparklets per pulse). This was plotted by the shaded bars in Fig. 8 *D*, and clearly does not match well to the experimental data. An excess of channels showed low sparklet frequencies, and a substantial population displayed higher-than-expected frequencies. Thus, channel properties are not stereotyped. Instead there is substantial channel-to-channel variation in open probability, even between closely adjacent channels monitored at the same time. A further question is whether part of this variability may arise through

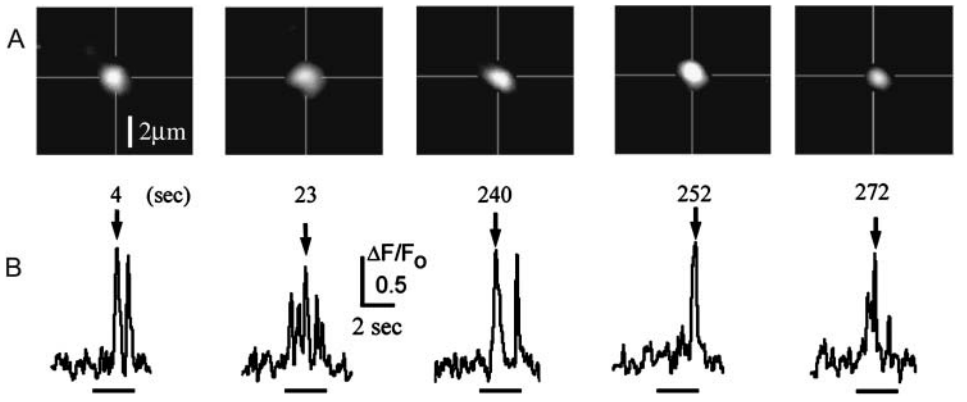

FIGURE 7 N-type Ca^{2+} channels are anchored in the oocyte membrane. Data were obtained from an oocyte stimulated by two trains of depolarizing pulses (−15 mV, train of five 3-s depolarizations at 0.1 Hz) separated by an interval of ~4 min. (*A*) Representative images of sparklets arising at a single channel at various times as indicated. Cross-hairs mark the initial position of the sparklet centroid. (*B*) Traces show fluorescence measurements throughout corresponding depolarizing pulses obtained from a region of interest (1 μm^2) centered on this channel.

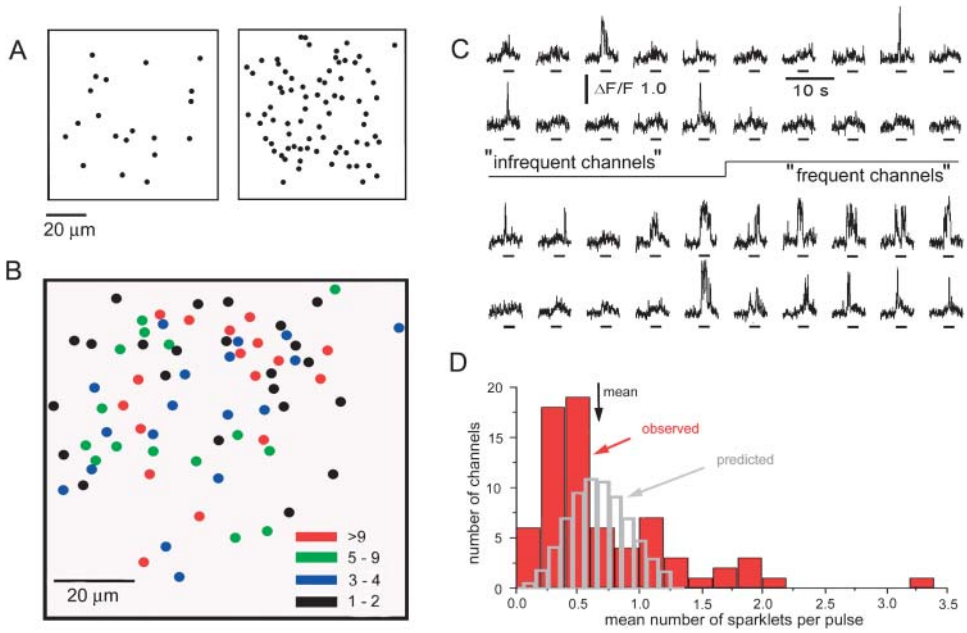

FIGURE 8 Spatial density of channels and differences in properties of channel within a small area of membrane. (*A*) Maps variation in channel density between two regions (60 × 60 μm) of the same oocyte membrane ~200-μm apart. Sparklets were evoked by a 3-s voltage pulse to 0 mV and dots mark locations where at least one sparklet was observed. (*B*) Diagram showing locations of all channels identified within a 60 × 60 μm region of membrane. The oocyte was stimulated by 10 successive depolarizing pulses to −10 mV. Colors denote the total number of sparklets observed at each site throughout the 10 pulses (*black* ≥ 2; *blue* 3–4; *green* 4–9; and *red* > 9). (*C*) Sample traces showing fluorescence records from selected sites, illustrating channels that showed relatively low frequencies of sparklets (*upper two records*), and relatively high frequencies (*lower two records*). (*D*) Red histogram shows the observed distribution of sparklet frequencies among the 72 channels illustrated in *B*. The mean number of sparklets per pulse was 0.685, and histogram bars indicate the number of channels that showed a given mean number of sparklets per pulse. Blue histogram shows the corresponding distribution expected from stochastic variability, assuming a Poisson distribution with mean of 0.685 events per pulse.

changes in activity of a given channel as a function of time. We did not find significant differences in sparklet frequencies between the first and last set of five depolarizing pulses of the recording epoch (only three out of 72 channels showed statistically significant differences; two-tailed *t*-test, $p = 0.05$); but the sample size was too small to exclude the possibility of nonstationary channel kinetics.

DISCUSSION

The patch-clamp recording technique (Neher and Sakmann, 1976) has revolutionized our understanding of single channel functioning by allowing electrophysiological recording of ion fluxes through individual channels. Nevertheless, it suffers some limitations—most notably, the lack of spatial information regarding channel localization within the cell membrane, and the inability to independently monitor activity of more than one channel at a time. We describe here a complementary optical approach, in which TIRFM is used to image Ca^{2+} flux through individual plasma membrane channels, thereby allowing simultaneous monitoring of the function and localization of multiple voltage-gated Ca^{2+} channels.

TIRFM images of cytosolic [Ca^{2+}] adjacent to the membrane of oocytes expressing N-type Ca^{2+} channels showed stochastic flashes (i.e., sparklets) during depolarizing pulses. Such events have previously been studied by wide-field imaging (Zou et al., 1999, 2002) and by line-scan confocal microscopy (Wang et al., 2001; Demuro and Parker, 2003), and almost certainly reflect Ca^{2+} flux through individual channels. Most notably, simultaneous patch-clamp recordings show a one-to-one correspondence between sparklets and single channel currents (Zou et al., 1999, 2002; Wang et al., 2001); the fluorescence signal mass of sparklets matches the expected single-channel Ca^{2+} flux (Demuro and Parker, 2003); and the kinetics of sparklets correspond well to channel gating properties measured electrophysiologically (Demuro and Parker, 2003).

To achieve good spatial and kinetic resolution, fluorescence measurements must be restricted to the close vicinity of the channel mouth where changes in [Ca^{2+}] are large and rapidly track the opening and closing of the channel. TIRFM thus provides a nearly ideal imaging technique for studying channels located in, or very close to the plasma membrane, owing to the extremely thin (~100 nm) optical section of the evanescent wave. By comparison, confocal microscopy has the advantage that Ca^{2+} signals can be recorded from intracellular channels at some depth into the cell but, although offering a lateral resolution similar to TIRFM (FWHM = ~400 nm), provides an inherently inferior optical section (~700 nm). Moreover, the necessity of scanning the laser spot limits the temporal resolution of confocal microscopes. Although specialized models operating at video and supra-video rates are available, most operate at only a few frames per second (fps). Confocal single-channel imaging studies to date have, therefore, utilized a line-scan mode which gives a time resolution as short as 1 ms, but provides spatial information in only one dimension and can monitor from

only a few channels at a time (Wang et al., 2001; Demuro and Parker, 2003). In contrast, the time resolution of TIRFM images is limited only by the frame rate of the camera which—although only 30 fps for the camera used here—can be as high as several hundred fps. A final advantage is that TIRFM is simpler and less expensive than confocal microscopy, and turnkey systems have recently become available from several microscope manufacturers.

A different approach to functional single channel imaging involves attaching a dye or fluorescent protein in a site-directed manner to a channel to reveal conformational changes associated with channel gating (Sonnleitner et al., 2002; Borisenko et al., 2003). This method has advantages for mechanistic studies in that it can reveal functional transitions that do not result in channel opening, but visualization of individual fluorophore molecules is beset by practical problems of weak signals (which may be hard to discriminate above cellular autofluorescence), fluorescence blinking, and irreversible photobleaching. On the other hand, imaging the behavior of single Ca^{2+} channels via the resulting Ca^{2+} flux provides a robust amplification. Thousands of Ca^{2+} ions pass during each opening of a channel (a current of 1 pA corresponds to $\sim$3000 ions ms^{-1}) and many of these will bind to indicator molecules that can each be excited to emit $>10^3$ photons ms^{-1}.

Imaging techniques can provide information that is inaccessible by electrophysiological means. For example, two-dimensional mapping of functional channels by TIRFM imaging should facilitate studies of channel clustering and diffusional motility. We find that N-type channels are rigidly anchored when expressed in the oocyte membrane but, although showing a patchy distribution over scales of tens of μm, do not appear to cluster. This may reflect specific differences between subtypes of Ca^{2+} channels, as YFP-tagged L-type channels heterologously expressed in HEK293 cells are mobile and aggregate (Harms et al., 2001). Moreover, imaging of Ca^{2+} flux permits measurements of channel function, not merely their localization, thereby making it possible to explore whether functional properties may be spatially regulated. Our results show that individual N-type channels within localized membrane regions display divergent opening probabilities, suggesting that they are differentially modulated. So far we have not found evidence for colocalization of channels with similar properties, but this may be evident in other systems owing, for example, to local differences in lipid composition or to spatially restricted signal transduction pathways.

We used *Xenopus* oocytes as a model cell system to facilitate development of TIRFM single-channel imaging technology, but this approach should be equally applicable to neurons and many other cell types. For example, TIRFM has been used to image localized domains of Ca^{2+} influx or liberation in chromaffin cells (Becherer et al., 2003), bipolar retinal neurons (Zenisek et al., 2003) and cardiac myocytes (Cleeman et al., 1997). The primary requirements are that the cell membrane must lie within $\sim$100 nm of a glass substrate—a condition readily fulfilled by acutely dissociated cells and by cells grown in culture on glass coverslips—and that the channel of interest must have an appreciable permeability to Ca^{2+}. Even though fluorescent indicators are available for other ions (e.g., Na^+, Cl^-) it is unlikely that these could be used to visualize single-channel flux, as the resulting concentration changes are orders-of-magnitude smaller than for Ca^{2+}. Nonetheless, numerous voltage- and ligand-gated channels are permeable to Ca^{2+}, and we have been able to record Ca^{2+} signals from single muscle nicotinic acetylcholine channels (A.D. and I.P., unpublished).

We anticipate TIRFM imaging will evolve as a powerful adjunct to the patch-clamp technique, as these methodologies have complementary advantages and limitations. Patch-clamping is unlikely to be surpassed for optimal resolution of channel kinetics and conductance, and inherently provides control of membrane voltage. On the other hand, imaging is less invasive, can simultaneously monitor $>$100 channels, and provides spatial information with submicrometer resolution. In addition to applications in basic research, TIRFM imaging holds promise for high-throughput screening of ion channel activity and may be more easily implemented than efforts to develop massively parallel arrays of patch-clamp electrodes (Sigworth and Klemic, 2002; Xu et al., 2001).

SUPPLEMENTARY MATERIAL

An online video supplement to this article can be found by visiting BJ Online at http://www.biophysj.org. This video shows sparklets imaged by TIRFM from a 60 $\times$ 60 μm membrane region of an oocyte expressing N-type Ca^{2+} channels. The membrane potential was stepped from -80 to -15 mV when indicated. Images were recorded at 30 frames s^{-1}, in Ringer's solution including 6 mM Ca^{2+}, and display increases in fluorescence ratio relative to the resting fluorescence before stimulation.

We thank Dr. Diane Lipscombe for providing Ca^{2+} channel clones.

This work was supported by National Institutes of Health grants GM48071 and GM65830.

REFERENCES

Allbritton, N. L., T. Meyer, and L. Stryer. 1992. Range of messenger action of calcium ion and inositol 1,4,5-trisphosphate. *Science*. 258:1812–1815.

Axelrod, D. 2003. Total internal reflection microscopy in cell biology. *Meth. Enzymol.* 361:1–33.

Becherer, U., T. Moser, W. Stuhmer, and M. Oheim. 2003. Calcium regulates exocytosis at the level of single vesicles. *Nat. Neurosci.* 6:846–853.

Borisenko, V., T. Lougheed, J. Hesse, E. Fureder-Kitzmuller, N. Fertig, J. C. Behrends, G. A. Woolley, and G. J. Schutz. 2003. Simultaneous

optical and electrical recording of single gramicidin channels. *Biophys. J.* 84:612–622.

Cleeman, L., G. DiMassa, and M. Morad. 1997. Ca^{2+} sparks within 200 nm of the sarcolemma of rat ventricular cells: evidence from total internal reflection microscopy. *Adv. Exp. Med. Biol.* 430:57–65.

Demuro, A., and I. Parker. 2003. Optical single-channel recording: imaging Ca^{2+} flux through individual N-type voltage-gated channels expressed in *Xenopus* oocytes. *Cell Calcium.* 34:499–599.

Edidin, M. 1987. Rotational and lateral diffusion of membrane proteins and lipids: phenomena and function. *Curr. Top. Membr. Trans.* 29:91–127.

Hamill, O. P., A. Marty, E. Neher, B. Sakmann, and F. J. Sigworth. 1981. Improved patch-clamp techniques for high-resolution current recording from cells and cell-free membrane patches. *Pflugers Arch.* 39:85–100.

Harms, G. S., L. Cognet, P. H. Lommerse, G. A. Blab, H. Kahr, R. Gamsjager, H. P. Spaink, N. M. Soldatov, C. Romanin, and T. Schmidt. 2001. Single-molecule imaging of L-type Ca^{2+} channels in live cells. *Biophys. J.* 81:2639–2646.

Lin, Z., S. Haus, J. Edgerton, and D. Lipscombe. 1997. Identification of functionally distinct isoforms of the N-type Ca^{2+} channel in rat sympathetic ganglia and brain. *Neuron.* 18:153–166.

Methfessel, C., V. Witzemann, T. Takahashi, M. Mishina, S. Numa, and B. Sakmann. 1986. Patch clamp measurements on *Xenopus laevis* oocytes: currents through endogenous channels and implanted acetylcholine receptor and sodium channels. *Pflugers Arch.* 407:577–588.

Miledi, R., and I. Parker. 1983. Chloride current induced by injection of calcium into *Xenopus* oocytes. *J. Physiol.* 357:173–183.

Neher, E., and B. Sakmann. 1976. Single-channel currents recorded from membrane of denervated frog muscle fibres. *Nature.* 260:799–802.

Parker, I. 2003. Photonics for biologists. *Meth. Enzymol.* 360:345–382.

Sigworth, F. J., and K. G. Klemic. 2002. Patch clamp on a chip. *Biophys. J.* 82:2831–2832.

Sonnleitner, A., and Y. Isacoff. 2003. Single ion channel imaging. *Meth. Enzymol.* 361:304–319.

Sonnleitner, A., L. M. Mannuzzu, S. E. Terakawa, and Y. Isacoff. 2002. Structural rearrangements in single ion channels detected optically in living cells. *Proc. Natl. Acad. Sci. USA.* 99:12759–12764.

Toomre, D., and D. J. Manstein. 2001. Lighting up the cell surface with evanescent wave microscopy. *Trends Cell Biol.* 11:298–303.

Wang, S. Q., L. S. Song, E. G. Lakatta, and H. Cheng. 2001. Ca^{2+} signalling between single L-type Ca^{2+} channels and ryanodine receptors in heart cells. *Nature.* 410:592–596.

Xu, J., X. B. Wang, B. Ensign, M. Li, L. Wu, A. Guia, and J. Xu. 2001. Ion-channel assay technologies: quo vadis? *Drug Discov. Today.* 6:1278–1287.

Zenisek, D., V. Davila, L. Wan, and W. Almers. 2003. Imaging calcium entry sites and ribbon structures in two presynaptic cells. *J. Neurosci.* 23:2538–2548.

Zou, H., L. M. Lifshitz, R. A. Tuft, K. E. Fogarty, and J. J. Singer. 1999. Imaging Ca^{2+} entering the cytoplasm through a single opening of a plasma membrane cation channel. *J. Gen. Physiol.* 114:575–588.

Zou, H., L. M. Lifshitz, R. A. Tuft, K. E. Fogarty, and J. J. Singer. 2002. Visualization of Ca^{2+} entry through single stretch-activated cation channels. *Proc. Natl. Acad. Sci. USA.* 99:6404–6409.